

Long-Tailed 3D Detection via 2D Late Fusion

Yechi Ma^{12*}, Neehar Peri^{3*}, Shuoquan Wei², Wei Hua², Deva Ramanan³, Yanan Li², Shu Kong⁴⁵

¹Zhejiang University, ²Zhejiang Lab, ³Carnegie Mellon University,

⁴University of Macau, ⁵Texas A&M University

Abstract: Long-Tailed 3D Object Detection (LT3D) addresses the problem of accurately detecting objects from both common and rare classes. Contemporary multi-modal detectors achieve low AP on rare-classes (e.g., CMT only achieves 9.4 AP on *stroller*), presumably because training detectors end-to-end with significant class imbalance is challenging. To address this limitation, we delve into a simple late-fusion framework that ensembles independently trained *uni-modal* LiDAR and RGB detectors. Importantly, such a late-fusion framework allows us to leverage large-scale uni-modal datasets (with more examples for rare classes) to train better uni-modal RGB detectors, unlike prevailing multimodal detectors that require paired multi-modal training data. Notably, our approach significantly improves rare-class detection by 7.2% over prior work. Further, we examine three critical components of our simple late-fusion approach from first principles and investigate whether to train 2D or 3D RGB detectors, whether to match RGB and LiDAR detections in 3D or the projected 2D image plane for fusion, and how to fuse matched detections. Extensive experiments reveal that 2D RGB detectors achieve better recognition accuracy for rare classes than 3D RGB detectors and matching on the 2D image plane mitigates depth estimation errors. Our late-fusion approach achieves 51.4 mAP on the established nuScenes LT3D benchmark, improving over prior work by 5.9 mAP!

Keywords: Long-Tailed 3D Detection, Multimodal Fusion, 2D Late Fusion

1 Introduction

3D object detection is an integral component of the autonomous vehicle (AV) perception stack [1, 2, 3, 4]. AVs must accurately detect objects from both common and rare classes for safe navigation. Although contemporary end-to-end trained multi-modal detectors have shown impressive performance on common classes (e.g., car and bus), they still struggle to detect rare classes (e.g., *stroller* and *debris*) due to limited paired training data in-the-tail. In this paper, we explore the established research problem of *Long-Tailed 3D Detection* (LT3D) [5], which focuses on achieving high accuracy on *both* common and rare classes.

Late-fusion requires *matching* and *fusing* uni-modal detections.

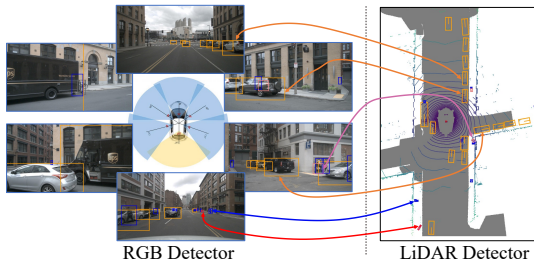


Figure 1: We explore a simple late-fusion framework for LT3D by ensembling RGB and LiDAR uni-modal detectors [5]. We rigorously examine three critical components (Fig. 2) from first principles and propose a simple method that fuses detections produced by 2D RGB and 3D LiDAR detectors. Our method achieves 51.4 mAP on the nuScenes [2] LT3D benchmark, significantly outperforming prior work [6] by 5.9 mAP (cf. Table 1).

*Equal Contribution.

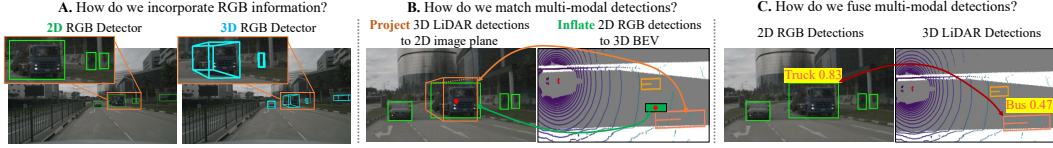


Figure 2: We examine three key components in the late-fusion of uni-modal RGB and LiDAR detectors from first principles: **A.** whether to train 2D or 3D RGB detectors, **B.** whether to match uni-modal detections on the 2D image plane or in the 3D bird’s-eye-view (BEV), and **C.** how to best fuse matched detections. Perhaps surprisingly, our exploration reveals that using 2D RGB detectors, matching on the 2D image plane, and combining calibrated scores with Bayesian fusion yields state-of-the-art LT3D performance, significantly outperforming end-to-end trained multi-modal detectors (cf. Table 1).

Status quo. LT3D is not well addressed by simply training state-of-the-art multi-modal detectors on both common and rare classes [5]. For example, BEVFusion [6], an end-to-end trained multi-modal transformer-based detector, only achieves 4.4 AP on the rare class *child* (cf. Table 7). In contrast, Peri et al. [5] finds that late-fusion (cf. Fig. 1) of monocular 3D RGB detections [7] and 3D LiDAR detections [8] improves rare class recognition, achieving state-of-the-art performance on the nuScenes [2] LT3D benchmark. Importantly, [5] demonstrates that ensembling uni-modal detectors is better suited for LT3D because 3D LiDAR detectors achieve high recall but struggle to correctly recognize rare classes, while RGB detectors excel at recognition but are unable to reliably estimate depth. This motivates our work, which investigates late-fusion from first principles.

The devil is in the details. To address LT3D, we delve into the simple late-fusion framework proposed by [5] (cf. Fig. 1) and study three critical design choices from first principles (cf. Fig. 2), including whether to train 2D or 3D RGB detectors, whether to match RGB and LiDAR detections in the 2D image plane or 3D bird’s-eye-view, and how to fuse matched detections.

First, we evaluate the impact of *using 2D versus 3D RGB detectors* for late-fusion, and find that the former is straightforward to train (without requiring expensive 3D cuboid annotations on RGB), can readily leverage external datasets that have 2D annotations (particularly improving rare class accuracy), and leads to significantly better LT3D performance (cf. Table 2). This is practically meaningful because annotating 2D boxes on RGB images is significantly cheaper than annotating 3D cuboids.

Next, we study the impact of matching 2D RGB detections and 3D LiDAR detections *on the 2D image plane versus in the 3D bird’s-eye-view (BEV)*. Matching detections in the 3D BEV requires inflating 2D detections to 3D using depth imputed from LiDAR points [9], introducing additional depth estimation errors. Instead, we demonstrate that projecting 3D LiDAR detections to the 2D image plane for matching is more robust (cf. Table 2).

Lastly, we explore *score calibration and Bayesian fusion* to combine matched detections. We find that proper score calibration improves rare class detection and enables probabilistic fusion [10] of LiDAR and RGB detections (cf. Table 3). Without score calibration, rare class detections are often suppressed by overlapping common class detections.

Contributions. We extensively study late-fusion from first principles, identify best practices including using 2D RGB detectors for fusion, and derive a simple method that incorporates the above insights to resoundingly outperform prior works on the established nuScenes and Argoverse 2 LT3D benchmarks. We rigorously ablate each component and justify our design choices. Importantly, the novelty of our work lies in our rigorous exploration of late-fusion in the context of long-tailed 3D detection.

2 Related Work

3D detection for autonomous vehicles (AVs) can be broadly classified based on input modalities: LiDAR-only, RGB-only, and multi-modal detectors. Recent work in 3D detection is inspired by prior work in 2D detection [11, 12, 13]. LiDAR-based detectors like PointPillars [14], CBGS [15],

and PVRCNN++ [16] adopt an SSD-like architecture [12] that regresses amodal bounding boxes from a BEV feature map. More recently, CenterPoint [8] adopts a center-regression loss inspired by [11]. Despite significant progress, LiDAR-based detectors often produce many false positives because it is difficult to distinguish foreground objects from background with sparse LiDAR points alone.

On the other hand, monocular RGB-based methods have gained increased interest in recent years due to low sensor cost and wide-spread adoption [17]. FCOS3D [7] extends FCOS [18] by additionally regressing the size, depth, and rotation for each detection. Recent methods such as BEVDet [19, 20] and BEVFormer [21] construct a BEV feature-map by estimating per-pixel depth [22]. PolarFormer [23] introduces a polar-coordinate transformation that improves near-field detection. Despite recent advances in LiDAR-only and RGB-only 3D detectors, multi-modal fusion is essential for LT3D [5] (detailed next). Importantly, using both RGB (for better recognition) and LiDAR (for better 3D localization) helps detect both rare and common classes. We delve into the late-fusion framework described in Fig. 1 to determine how to effectively fuse RGB and LiDAR uni-modal detectors for LT3D (cf. Fig. 2).

Multimodal fusion for 3D object detection is an active research area. Popular approaches can be categorized into input-fusion, feature-fusion, and late-fusion. Input-fusion methods typically augment LiDAR points using image-level features. For example, PointPainting [24] projects LiDAR points onto a semantic segmentation mask and appends corresponding class scores to each point. MVP [25] densifies regions of LiDAR sweeps that correspond with objects in semantic segmentation masks. Frustum PointNets [26] and SRDL [27] leverage 2D RGB detections to regress 3D bounding boxes for LiDAR points within the 2D detection frustum using PointNets [28].

Recent works show that feature-fusion can be more effective than input-fusion. PointFusion [29] fuses global image and point-cloud features prior to detection and MSMDFusion [30] fuses LiDAR and RGB features at multiple scales. TransFusion [31] and BEVFusion [6] fuse features in the BEV space using multi-head attention. Despite the success of transformers for detecting common objects, [5] finds that TransFusion struggles to detect rare classes, as the transformer architecture (adopted in TransFusion and BEVFusion) suffers from limited paired RGB-LiDAR training data in the long tail. For transformers to work well in practice, they may require diverse, large-scale training datasets [32, 33, 34]. Therefore, we opt to study late-fusion of uni-modal detectors, which does not require paired RGB-LiDAR training data.

CLOCs [35] is a late-fusion method that learns a standalone fusion network to merge RGB and LiDAR detections, showing promising results for 3D detection. More recently, [5] introduces a simple non-learned filtering algorithm that effectively removes false-positive LiDAR-detections that are far away from any 3D RGB detections. We delve into this simple late-fusion framework and present a method that significantly outperforms prior methods for LT3D.

Long-tailed detection is not unique to the AV domain and has been well studied in 2D [36]. Existing methods propose reweighting losses [37, 38, 39, 40, 41], rebalancing data sampling [42, 43, 44, 15], balancing gradients computed from imbalanced classes [45], and balancing network weights [46]. CBGS [15] explicitly addresses rare-class 3D detection by up-sampling LiDAR sweeps with instances of rare classes, and pasting rare objects copied from different scenes. More recently, [47] adopts data augmentation via sampling, and [48] uses active learning and hard example mining to obtain more data for rare classes. LT3D presents distinct opportunities and challenges compared to 2D long-tailed detection because LiDAR sensors offer direct geometric and ego-motion cues that are difficult to extract from 2D images.

3 Late-Fusion of RGB and LiDAR Detections

We first analyze different ways of incorporating RGB information in Sec. 3.1, present a simple algorithm for matching RGB and LiDAR detections in Sec. 3.2, and finally describe score calibration and probabilistic fusion in Sec. 3.3.

3.1 How Do We Incorporate RGB Information?

Although LiDAR offers accurate localization, LiDAR-only detectors struggle to distinguish foreground objects from background using sparse LiDAR alone. RGB images provide complementary information that is essential for identifying objects and disambiguating those that are geometrically similar in point clouds but semantically different in images (e.g., construction worker vs. police officer). Although prior works address late-fusion, they combine *3D RGB detectors* with 3D LiDAR detections [5]. In contrast, we find that *ensembling 2D RGB detectors* with 3D LiDAR detectors yields significantly better LT3D performance. We present insights on why using 2D detectors to incorporate RGB information yields better performance below, and ablate the impact of using 2D versus 3D RGB detectors for late-fusion in Table 2.

2D RGB detectors are more mature. 2D object detection is a fundamental problem in computer vision [49, 50, 51] that has matured in recent years and model trade-offs are well understood [51, 52, 53]. In this work, we consider two state-of-the-art 2D RGB detectors, YOLOV7 [54] and DINO [55]. YOLOV7 is a real-time detector that identifies a number of training tricks that nearly doubles the inference efficiency over prior work without sacrificing performance. DINO (not to be confused with the foundational feature extractor DINO [56]) is a recent transformer-based detector that improves upon DETR [13] using denoising anchor boxes. As 2D detectors do not make 3D predictions (e.g., depth and rotation), understanding how to best leverage them in the context of long-tailed 3D detection is a key challenge. We address this in Section 3.2.

2D RGB detectors can be trained with more diverse data. Training 2D RGB detectors only requires *2D bounding box* annotations, which are significantly cheaper to collect than 3D cuboids used for training 3D RGB detectors [7, 23]. Since annotating 3D amodal cuboids is both expensive and non-trivial (compared to bounding-box annotations for 2D detection), datasets for monocular 3D RGB detection are considerably smaller and less diverse than their 2D detection counterparts. For example, nuScenes [2] (published in 2020) annotates 144K RGB images of 23 classes using 3D cuboids, while COCO [50] (an early 2D detection dataset published in 2014) annotates 330K images of 80 classes using 2D bounding boxes. This allows us to pretrain 2D RGB detectors on significantly larger, more diverse, publicly available datasets [57, 58, 59, 60, 61]. We demonstrate that leveraging existing 2D detection datasets helps train stronger 2D detectors “for free”, further improving LT3D performance (cf. Fig. 7).

3.2 How Do We Match Uni-Modal Detections?

Finding correspondence between two sets of RGB and LiDAR uni-modal detections is an essential step in the late-fusion framework (cf. Fig. 2B). Prior work [5] matches 3D RGB and 3D LiDAR detections using center distance in the bird’s-eye-view (BEV) plane. However, precisely matching detections is difficult due to depth estimation errors from 3D RGB detectors. Instead, we opt to match *2D RGB* and 3D LiDAR detections. Prior work attempts to inflate 2D detections to the 3D BEV (using LiDAR points [9]), but we find that matching inflated 2D detections in the 3D BEV suffers from many of the same limitations as 3D RGB detections. Importantly, inflated 2D RGB detections impute additional depth estimation errors and reduce overall match quality. In contrast, we match multi-modal detections by projecting 3D LiDAR detections onto the 2D image plane, avoiding additional noise due to imprecise depth estimates. We ablate the impact of matching in the 3D BEV versus on the 2D image plane in Table 2, and present our 2D matching algorithm below.

Spatial matching on the 2D image plane. Using the available sensor extrinsics, we project 3D LiDAR detections onto the 2D image plane. We then use the IoU metric to determine overlap between (projected) LiDAR and 2D RGB detections. A 2D RGB detection and a (projected) 3D LiDAR detection are considered a match if their IoU is greater than a fixed threshold. Although conceptually simple, we find that it works significantly better than using center distance to match detections in the 3D BEV (cf. bottom two rows in Table 2). Spatially matching uni-modal detections using 2D IoU yields three categories of detections: matched detections, unmatched RGB detections

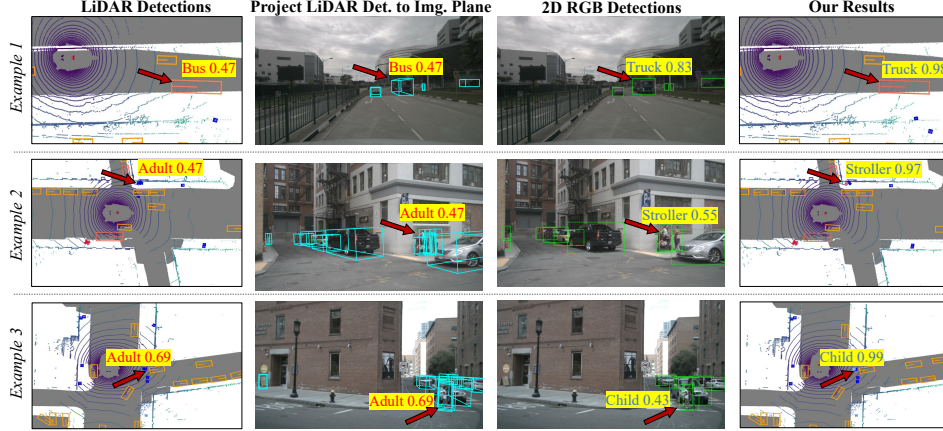


Figure 3: Three examples demonstrate how ensembling 2D RGB detections (from DINO [55]) and 3D LiDAR detections (from CenterPoint [8]) improves LT3D performance. In all examples, our method is able to correctly relabel detections which are geometrically similar (w.r.t size and shape) in LiDAR but are visually distinct in RGB, such as bus-vs-truck, adult-vs-stroller, and adult-vs-child.

(that do not have corresponding LiDAR detections), and unmatched LiDAR detections (that do not have corresponding RGB detections).

Handling unmatched detections. We remove unmatched 2D RGB detections, positing that any unmatched RGB detections are likely to be false positives given that LiDAR detectors tend to yield high recall [5]. Further, accurately inflating 2D RGB detections to 3D remains challenging. For unmatched 3D LiDAR detections, we down-weight their detection confidence scores by w (inspired by SoftNMS [62]). We optimize for w by grid search on a val-set, and set $w = 0.4$.

3.3 How Do We Fuse Matched Detections?

As illustrated by Fig. 2C, detections may match spatially but not semantically. To address this, we propose a semantic matching heuristic to better fuse LiDAR and RGB detections. Given a pair of spatially matched RGB and LiDAR detections, we consider two cases: matched detections with semantic disagreement (e.g. RGB and LiDAR predict different classes), and matched detections with semantic agreement (e.g. RGB and LiDAR predict the same class).

Addressing semantic disagreement between modalities. If both modalities predict different semantic classes, we use the confidence score and class label of the RGB-based detection and the 3D box extent from the LiDAR-based detection. Intuitively, RGB detectors can predict semantics more reliably from high resolution images than LiDAR-only detectors. This helps correct misclassifications of geometrically similar, but semantically different objects produced by the 3D LiDAR detector, as shown in Fig. 3. Importantly, prior late fusion methods like CLOCS [35] only perform late-fusion on matched predictions with semantic agreement and do not fix misclassifications. We find that this is critical for improving rare class performance.

If both modalities predict the same semantic class, we perform score fusion and probabilistic ensembling [63] as described below. Note that the confidence scores of RGB and LiDAR detections are not directly comparable by default. Specifically, we find that LiDAR-based detectors are often under-confident because it is difficult to distinguish foreground-vs-background using sparse LiDAR alone. Therefore, score calibration is crucial for fusion. Below, we explore score calibration of RGB (x_{RGB}) and LiDAR (x_{LiDAR}) detections.

Score calibration. In this work, we calibrate detection confidences per model by tuning a temperature τ_c for the logit score of class c on a val-set before applying a sigmoid transform [64, 63], i.e., $\text{sigmoid}(\text{logit}_c/\tau_c)$. Optimally tuning per-class τ_c is computationally expensive as it requires tuning for all classes at the same time. Instead, we choose to greedily tune each τ_c , optimizing per-class AP on a val-set for each class progressively ordered by their cardinalities. It is worth noting that this

score calibration is only performed once in training and tuned τ_c and $p(c)$ do not need further optimization during inference. Importantly, score calibration does not increase runtime or complexity.

Probabilistic ensembling. We assume independent class prior $p(c)$ and conditional independence given the class label c [63], i.e., $p(x_{\text{RGB}}, x_{\text{LiDAR}}|c) = p(x_{\text{RGB}}|c)p(x_{\text{LiDAR}}|c)$. We compute the final score as

$$\begin{aligned} p(c|x_{\text{RGB}}, x_{\text{LiDAR}}) &= p(x_{\text{RGB}}, x_{\text{LiDAR}}|c)p(c) / p(x_{\text{RGB}}, x_{\text{LiDAR}}) \\ &\propto p(x_{\text{RGB}}, x_{\text{LiDAR}}|c)p(c) \\ &\propto p(x_{\text{RGB}}|c)p(x_{\text{LiDAR}}|c)p(c) \\ &\propto p(c|x_{\text{RGB}})p(c|x_{\text{LiDAR}}) / p(c) \end{aligned}$$

where $p(c|x_{\text{RGB}})$ and $p(c|x_{\text{LiDAR}})$ are the posteriors after calibration. Unlike balanced class distribution studied in [63], in the long-tailed scenario, $p(c)$ can significantly impact the final LT3D performance. To maximize performance, the optimal tuning practice is to jointly tune all class priors $p(c)$ altogether, which is computationally expensive. Hence, similar to score calibration, we greedily tune $p(c)$, one by one ordered by class cardinality. Similar to score calibration, probabilistic ensembling does not increase inference time or complexity.

4 Experiments

In this section, we conduct extensive experiments to evaluate our proposed approach. We compare our late-fusion approach with prior work and present a detailed ablation study that further addresses the three motivating questions in Fig. 2. We find that our proposed approach improves over prior works by 5.9% mAP, notably improving by 7.2% on rare classes (Table 1). We include our code in the supplementary material, and will publically release it to facilitate future work.

Datasets. We study LT3D using the well-established nuScenes dataset [2]. We follow the suggested protocol in [5], using all 18 long-tail categories for benchmarking. Moreover, we use the nuImages dataset [2] as an external 2D annotated data source to study how using additional data to train better 2D RGB detectors improves late-fusion performance. Lastly, we also evaluate our approach on the Argoverse 2 dataset [3] in the supplement, and find that our conclusions hold across datasets. Note that other datasets such as KITTI [1] and Waymo [4] do not support the study of LT3D as they only annotate three common classes.

Table 1: **Benchmarking various approaches for LT3D on the nuScenes dataset** (measured by mAP). We denote the modalities used in each method: C for RGB camera and L for LiDAR. Recall that our approach fuses 3D LiDAR and 2D RGB detections (produced by CenterPoint and DINO, respectively) on the 2D image plane with score calibration and probabilistic ensembling. Our frustratingly simple approach performs the best averaged across *all* common and rare classes, notably outperforming end-to-end multi-modal methods such as BEVFusion [6], DeepInteraction [65], and CMT [66]. Note that “CenterPoint + FCOS3D” is a baseline late-fusion method proposed by [5], which underperforms our late-fusion approach. Importantly, our approach nearly doubles the detection performance achieved by prior work on classes with **few** examples!

Method	Modality	All	Many	Medium	Few
FCOS3D [7]	C	20.9	39.0	23.3	2.9
BEVFormer[21]	C	27.3	52.3	31.6	1.4
PolarFormer [23]	C	28.0	54.0	31.6	2.2
CenterPoint [8]	L	40.4	77.1	45.1	4.3
TransFusion-L [31]	L	38.5	68.5	42.8	8.4
BEVFusion-L [6]	L	42.5	72.5	48.0	10.6
CMT-L [66]	L	34.7	73.4	35.9	1.1
CenterPoint [8] + RCNN [67]	C+L	34.0	64.8	37.5	4.3
CLOCS [35]	C+L	40.0	68.2	45.7	10.0
TransFusion [31]	C+L	39.8	73.9	41.2	9.8
BEVFusion [6]	C+L	45.5	75.5	52.0	12.8
DeepInteraction [65]	C+L	43.7	76.2	51.1	7.9
CMT [66]	C+L	44.4	79.9	53.0	4.8
CenterPoint + FCOS3D [5]	C+L	43.6	77.1	49.0	9.4
CenterPoint + DINO Det. (Ours)	C+L	51.4	77.9	59.4	20.0

Metrics. Mean average precision (mAP) is an established metric for object detection [50]. For 3D detection, a true positive (TP) is defined as a detection that has a center distance within a distance threshold on the ground-plane to a ground-truth annotation [2]. mAP computes the mean of AP over all classes, where per-class AP is the area under the precision-recall curve drawn with distance thresholds of [0.5, 1, 2, 4] meters. We report the metrics for three groups of classes based on their cardinalities: Many (>50k training instances per class), Medium (5k~50k), and Few (<5k). Following [5], we use the official nuScenes train-set for training and report numbers on the val-set because the official test-set does not evaluate on all 18 LT3D classes.

4.1 Comparison to the State-of-the-Art Methods

We compare our late-fusion approach against prior work in Table 1, and present qualitative results in Fig. 3. We adapt existing methods (which were previously trained on 10 classes in nuScenes) for LT3D by retraining them on all 18 classes.

CenterPoint [8], a popular LiDAR-only 3D detector, is unable to detect rare objects, achieving just 3.5% AP on classes with few examples. This is expected as it is difficult to identify rare objects from sparse LiDAR points alone. Perhaps surprisingly, the transformer-based 3D LiDAR detector BEVFusion-L performs considerably better on rare classes, achieving 10.6% AP. However, BEVFusion-L performs 3.9% worse than CenterPoint on classes with many examples. We posit that limited training data in-the-tail and class imbalance makes it difficult to learn generalizable features. In contrast, BEVFusion [21], which is an end-to-end trained multi-modal method, performs 3.0% better than the LiDAR-only variant (BEVFusion-L), confirming the benefit of using both RGB and LiDAR for LT3D. Next, we implement a simple baseline (termed “CenterPoint + RCNN”) that trains a region-based CNN (RCNN) [67] classifier on cropped regions corresponding to projected 3D detections. Notably, it underperforms CenterPoint by 6.4%, presumably because learning classifiers on cropped regions does not exploit contextual information and leads to worse classification accuracy. Peri et. al. [5] introduces a simple filtering algorithm (termed “CenterPoint + FCOS3D”), which keeps CenterPoint detections that are close (based on center distance) to monocular 3D RGB detections produced by FCOS3D in the BEV and discards all other LiDAR predictions. Given the success of this simple approach, we study this late-fusion paradigm further. Lastly, we re-implement CLOCS [35] by fusing detections from DINO and CenterPoint respectively. Note that CLOCS only fuses predictions from the same class, which prevents re-labeling misclassified LiDAR detections.

4.2 Ablation Study

In this section, we design a set of experiments to study the trade-off between using 2D and 3D RGB detectors, and matching in the 2D image and 3D BEV plane (cf. Table 2). Further, we examine the impact of using additional data and study different fusion strategies (cf. Table 3).

Table 2: Fusing uni-modal detections in the 3D BEV vs. on the 2D image plane. We evaluate the impact of fusing 3D LiDAR detections (from CenterPoint trained with hierarchical loss [5]) with 2D RGB and 3D RGB detections in both the 3D BEV and 2D image plane. We match and filter detections in the 3D BEV using center distance as proposed by [5], and match and filter detections in the 2D image plane using IoU. Following [9], we inflate 2D detections to the 3D BEV using LiDAR points within the box frustum. We project 3D detections to the 2D plane using provided sensor extrinsics. We find that matching 3D RGB detections in the 3D BEV and in the 2D image plane yields similar results. Unsurprisingly, inflating 2D RGB detections for matching in the 3D BEV performs worse than matching 3D RGB detections in the 3D BEV. In contrast, filtering LiDAR-based detections using 2D detections in the 2D image plane (bottom right panel) significantly improves performance for classes with medium and few examples by >10 mAP. This suggests that 2D detectors achieve better detection performance compared to 3D RGB detectors. We further verify this in Table 9.

Method	Fusion in 3D BEV				Fusion on 2D Image Plane			
	All	Many	Medium	Few	All	Many	Medium	Few
CenterPoint	40.4	77.1	45.1	4.3	40.4	77.1	45.1	4.3
+ FCOS3D [7]	42.9	76.6	48.7	8.1	42.6	75.0	49.4	7.7
+ BEVFormer [21]	43.2	76.9	50.8	6.3	42.8	75.2	51.4	5.7
+ PolarFormer [23]	42.8	76.8	50.0	6.1	42.6	75.1	51.1	5.6
+ YOLOV7 [54]	40.1	76.1	43.8	5.8	45.7	77.1	52.8	11.2
+ DINO [55]	40.3	76.2	44.1	5.9	49.5	77.4	57.7	16.7

Table 3: **Ablation on late-fusion.** Our analysis confirms that 2D RGB detectors are better suited for late-fusion, matching projected 3D LiDAR detections on the 2D image-plane outperforms matching 2D RGB detections inflated to the 3D BEV, and score calibration prior and probabilistic fusion improve performance. Importantly, a majority of our performance improvement can be attributed to matching and filtering on the 2D image plane with DINO. In addition, training with external data further improves rare class detection by 4.2%.

Method	Δ	All	Many	Medium	Few
CenterPoint w/ Hierarchy [5]		40.4	77.1	45.1	4.3
+ 2D Img. Filtering w/ DINO Det.	+7.5	47.9	77.1	55.8	14.4
+ External Data	+1.9	49.8	77.1	57.1	18.6
+ Score Calibration	+0.7	50.5	77.8	58.2	18.7
+ Probabilistic Ensembling	+0.9	51.4	77.9	59.4	20.0

How do we incorporate RGB information? Although LiDAR-based detectors are widely adopted for 3D detection, they produce many high-scoring false positives (FPs) for rare classes due to misclassification. We focus on removing such FPs using an RGB-based detector by leveraging two insights: LiDAR-based 3D detections are accurate w.r.t 3D localization and yield high recall (though classification is poor), and RGB-based detections are accurate w.r.t recognition (though 3D localization is poor). We incorporate RGB information by matching and filtering 3D LiDAR detections with RGB-based detections. We evaluate the impact of using 2D RGB-based detectors (e.g., YOLOV7 and DINO Det.) versus 3D RGB-based detectors (e.g., FCOS3D, BEVFormer, PolarFormer) in Table 2. We also analyze the impact of matching LiDAR detections with 2D RGB detections in the 3D BEV and 2D image plane. As shown in Table 2, matching LiDAR detections with 2D RGB detections in the 2D image plane (bottom right) performs best.

How do we match detections from uni-modal detectors? To match and filter LiDAR and RGB detections in the 3D BEV, we follow the procedure introduced by [5]. For each RGB-based detection, we keep LiDAR-based detections within a radius of m meters and remove all the others that are not close to any RGB-based detections. This works well for 3D RGB detections. Late fusion with FCOS3D, BEVFormer, and PolarFormer improves over the LiDAR-only model by 2% averaged over all classes (cf. Table 2). Unsurprisingly, we find that matching inflated 2D RGB detections in the 3D BEV performs worse than matching 3D RGB detections in the 3D BEV, notably achieving marginally lower accuracy than the LiDAR-only baseline.

Table 2 shows that projecting LiDAR detections on the 2D image plane and fusing them with 2D RGB detections significantly improves performance for classes with medium and few examples by more than 10% mAP. In contrast, projecting 3D RGB detections for matching on the 2D image plane performs worse than matching 2D RGB detections on the 2D image plane, suggesting that 2D detectors achieve better recognition performance than 3D RGB detectors (cf. Table 9).

How do we fuse matched detections? Prior to fusion, we first calibrate the scores of LiDAR and RGB detections to ensure that they are comparable. This improves accuracy by 0.7% averaged over all classes, notably improving performance for classes with a medium number of examples (cf. Table 3). For probabilistic ensembling, we use Bayesian fusion to reason about the final score of matched detections. Concretely, if two matched detections fire in the same place, the fused score should be higher than the individual scores because there is twice the evidence of an object at that particular spatial location. As shown in Table 3, this further improves accuracy by 0.9 mAP.

5 Conclusion

In this paper, we present a detailed exploration of late-fusion for long-tailed 3D detection. We find that 2D RGB detectors are better suited for late-fusion, matching projected 3D LiDAR detections on the 2D image-plane outperforms matching 2D RGB detections inflated to the 3D BEV, and score calibration and probabilistic fusion improve performance. Our simple late-fusion approach achieves state-of-the-art performance, improving over prior work by 5.9% mAP.

References

- [1] A. Geiger, P. Lenz, and R. Urtasun. Are we ready for autonomous driving? the kitti vision benchmark suite. In *CVPR*, 2012.
- [2] H. Caesar, V. Bankiti, A. H. Lang, S. Vora, V. E. Liong, Q. Xu, A. Krishnan, Y. Pan, G. Baldan, and O. Beijbom. nuscenes: A multimodal dataset for autonomous driving. In *Proceedings of the CVPR*, 2020.
- [3] B. Wilson, W. Qi, T. Agarwal, J. Lambert, J. Singh, S. Khandelwal, B. Pan, R. Kumar, A. Hartnett, J. K. Pontes, D. Ramanan, P. Carr, and J. Hays. Argoverse 2: Next generation datasets for self-driving perception and forecasting. In *Neural Information Processing Systems Datasets and Benchmarks Track*, 2021.
- [4] P. Sun, H. Kretzschmar, X. Dotiwalla, A. Chouard, V. Patnaik, P. Tsui, J. Guo, Y. Zhou, Y. Chai, B. Caine, V. Vasudevan, W. Han, J. Ngiam, H. Zhao, A. Timofeev, S. Ettinger, M. Krivokon, A. Gao, A. Joshi, Y. Zhang, J. Shlens, Z. Chen, and D. Anguelov. Scalability in perception for autonomous driving: Waymo open dataset. In *CVPR (CVPR)*, 2020.
- [5] N. Peri, A. Dave, D. Ramanan, and S. Kong. Towards long-tailed 3d detection. In *Conference on Robot Learning (CoRL)*, 2022.
- [6] Z. Liu, H. Tang, A. Amini, X. Yang, H. Mao, D. Rus, and S. Han. Bevfusion: Multi-task multi-sensor fusion with unified bird’s-eye view representation. *arXiv:2205.13542*, 2022.
- [7] T. Wang, X. Zhu, J. Pang, and D. Lin. FCOS3D: fully convolutional one-stage monocular 3d object detection. In *ICCV*, 2021.
- [8] T. Yin, X. Zhou, and P. Krahenbuhl. Center-based 3d object detection and tracking. In *CVPR*, 2021.
- [9] B. Wilson, Z. Kira, and J. Hays. 3d for free: Crossmodal transfer learning using hd maps. *arXiv:2008.10592*, 2020.
- [10] H. Chiu, A. Prioletti, J. Li, and J. Bohg. Probabilistic 3d multi-object tracking for autonomous driving. *CoRR abs/2001.05673*, 2020.
- [11] X. Zhou, V. Koltun, and P. Krähenbühl. Tracking objects as points. *CoRR abs/2004.01177*, 2020.
- [12] W. Liu, D. Anguelov, D. Erhan, C. Szegedy, S. Reed, C.-Y. Fu, and A. C. Berg. Ssd: Single shot multibox detector. In *ECCV*, 2016.
- [13] N. Carion, F. Massa, G. Synnaeve, N. Usunier, A. Kirillov, and S. Zagoruyko. End-to-end object detection with transformers. In *ECCV*, 2020.
- [14] A. H. Lang, S. Vora, H. Caesar, L. Zhou, J. Yang, and O. Beijbom. Pointpillars: Fast encoders for object detection from point clouds. In *CVPR*, 2019.
- [15] B. Zhu, Z. Jiang, X. Zhou, Z. Li, and G. Yu. Class-balanced grouping and sampling for point cloud 3d object detection. *arXiv:1908.09492*, 2019.
- [16] S. Shi, L. Jiang, J. Deng, Z. Wang, C. Guo, J. Shi, X. Wang, and H. Li. Pv-rcnn++: Point-voxel feature set abstraction with local vector representation for 3d object detection. *International Journal of Computer Vision*, pages 1–21, 2022.
- [17] Y. Hu, J. Yang, L. Chen, K. Li, C. Sima, X. Zhu, S. Chai, S. Du, T. Lin, W. Wang, L. Lu, X. Jia, Q. Liu, J. Dai, Y. Qiao, and H. Li. Planning-oriented autonomous driving. In *CVPR*, 2023.

- [18] Z. Tian, C. Shen, H. Chen, and T. He. Fcos: Fully convolutional one-stage object detection. In *Proceedings of the IEEE/CVF international conference on computer vision*, pages 9627–9636, 2019.
- [19] J. Huang, G. Huang, Z. Zhu, and D. Du. Bevdet: High-performance multi-camera 3d object detection in bird-eye-view. *arXiv:2112.11790*, 2021.
- [20] J. Huang and G. Huang. Bevdet4d: Exploit temporal cues in multi-camera 3d object detection. *arXiv:2203.17054*, 2022.
- [21] Z. Li, W. Wang, H. Li, E. Xie, C. Sima, T. Lu, Y. Qiao, and J. Dai. Bevformer: Learning bird’s-eye-view representation from multi-camera images via spatiotemporal transformers. In *ECCV*, 2022.
- [22] J. Philion and S. Fidler. Lift, splat, shoot: Encoding images from arbitrary camera rigs by implicitly unprojecting to 3d. In *ECCV*, 2020.
- [23] Y. Jiang, L. Zhang, Z. Miao, X. Zhu, J. Gao, W. Hu, and Y.-G. Jiang. Polarformer: Multi-camera 3d object detection with polar transformers. *arXiv:2206.15398*, 2022.
- [24] S. Vora, A. H. Lang, B. Helou, and O. Beijbom. Pointpainting: Sequential fusion for 3d object detection. In *CVPR*, 2020.
- [25] T. Yin, X. Zhou, and P. Krähenbühl. Multimodal virtual point 3d detection. *NeurIPS*, 2021.
- [26] C. R. Qi, W. Liu, C. Wu, H. Su, and L. J. Guibas. Frustum pointnets for 3d object detection from rgb-d data. In *IEEE conference on computer vision and pattern recognition*, 2018.
- [27] Q. He, Z. Wang, H. Zeng, Y. Zeng, Y. Liu, S. Liu, and B. Zeng. Stereo rgb and deeper lidar-based network for 3d object detection in autonomous driving. *IEEE Transactions on Intelligent Transportation Systems*, 24(1):152–162, 2022.
- [28] C. R. Qi, H. Su, K. Mo, and L. J. Guibas. Pointnet: Deep learning on point sets for 3d classification and segmentation. In *Proceedings of the IEEE conference on computer vision and pattern recognition*, pages 652–660, 2017.
- [29] D. Xu, D. Anguelov, and A. Jain. Pointfusion: Deep sensor fusion for 3d bounding box estimation. In *IEEE conference on computer vision and pattern recognition*, 2018.
- [30] Y. Jiao, Z. Jie, S. Chen, J. Chen, X. Wei, L. Ma, and Y.-G. Jiang. Msmdfusion: Fusing lidar and camera at multiple scales with multi-depth seeds for 3d object detection. *arXiv:2209.03102*, 2022.
- [31] X. Bai, Z. Hu, X. Zhu, Q. Huang, Y. Chen, H. Fu, and C.-L. Tai. Transfusion: Robust lidar-camera fusion for 3d object detection with transformers. In *CVPR*, 2022.
- [32] A. Dosovitskiy, L. Beyer, A. Kolesnikov, D. Weissenborn, X. Zhai, T. Unterthiner, M. Dehghani, M. Minderer, G. Heigold, S. Gelly, et al. An image is worth 16x16 words: Transformers for image recognition at scale. *arXiv:2010.11929*, 2020.
- [33] A. Radford, J. W. Kim, C. Hallacy, A. Ramesh, G. Goh, S. Agarwal, G. Sastry, A. Askell, P. Mishkin, J. Clark, et al. Learning transferable visual models from natural language supervision. In *International conference on machine learning*, pages 8748–8763. PMLR, 2021.
- [34] Y. Li, A. W. Yu, T. Meng, B. Caine, J. Ngiam, D. Peng, J. Shen, Y. Lu, D. Zhou, Q. V. Le, et al. Deepfusion: Lidar-camera deep fusion for multi-modal 3d object detection. In *CVPR*, 2022.
- [35] S. Pang, D. Morris, and H. Radha. Clocs: Camera-lidar object candidates fusion for 3d object detection. In *IROS*, 2020.

- [36] A. Gupta, P. Dollar, and R. Girshick. Lvis: A dataset for large vocabulary instance segmentation. In *CVPR*, 2019.
- [37] Y. Cui, M. Jia, T.-Y. Lin, Y. Song, and S. Belongie. Class-balanced loss based on effective number of samples. In *CVPR*, 2019.
- [38] S. H. Khan, M. Hayat, M. Bennamoun, F. A. Sohel, and R. Togneri. Cost-sensitive learning of deep feature representations from imbalanced data. *IEEE transactions on neural networks and learning systems*, 29(8):3573–3587, 2017.
- [39] K. Cao, C. Wei, A. Gaidon, N. Arechiga, and T. Ma. Learning imbalanced datasets with label-distribution-aware margin loss. In *NeurIPS*, 2019.
- [40] C. Huang, Y. Li, C. C. Loy, and X. Tang. Deep imbalanced learning for face recognition and attribute prediction. *PAMI*, 42(11):2781–2794, 2019.
- [41] S. Zhang, Z. Li, S. Yan, X. He, and J. Sun. Distribution alignment: A unified framework for long-tail visual recognition. In *CVPR*, 2021.
- [42] C. Drummond, R. C. Holte, et al. C4. 5, class imbalance, and cost sensitivity: why under-sampling beats over-sampling. In *Workshop on learning from imbalanced datasets II*, 2003.
- [43] N. V. Chawla, K. W. Bowyer, L. O. Hall, and W. P. Kegelmeyer. Smote: synthetic minority over-sampling technique. *Journal of Artificial Intelligence Research*, 16:321–357, 2002.
- [44] H. Han, W.-Y. Wang, and B.-H. Mao. Borderline-smote: a new over-sampling method in imbalanced data sets learning. In *International Conference on Intelligent Computing*, 2005.
- [45] K. Tang, J. Huang, and H. Zhang. Long-tailed classification by keeping the good and removing the bad momentum causal effect. In *NeurIPS*, 2020.
- [46] S. Alshammari, Y.-X. Wang, D. Ramanan, and S. Kong. Long-tailed recognition via weight balancing. In *CVPR*, 2022.
- [47] D. Lee and J. Kim. Resolving class imbalance for lidar-based object detector by dynamic weight average and contextual ground truth sampling. In *Proceedings of the IEEE/CVF Winter Conference on Applications of Computer Vision*, pages 682–691, 2023.
- [48] C. M. Jiang, M. Najibi, C. R. Qi, Y. Zhou, and D. Anguelov. Improving the intra-class long-tail in 3d detection via rare example mining. In *European Conference on Computer Vision*, pages 158–175. Springer, 2022.
- [49] P. F. Felzenszwalb, R. B. Girshick, D. McAllester, and D. Ramanan. Object detection with discriminatively trained part-based models. *IEEE transactions on pattern analysis and machine intelligence*, 32(9):1627–1645, 2009.
- [50] T. Lin, M. Maire, S. J. Belongie, J. Hays, P. Perona, D. Ramanan, P. Dollár, and C. L. Zitnick. Microsoft COCO: common objects in context. In *ECCV*, 2014.
- [51] S. Ren, K. He, R. Girshick, and J. Sun. Faster r-cnn: Towards real-time object detection with region proposal networks. In *Advances in Neural Information Processing Systems*, 2015.
- [52] J. Redmon, S. Divvala, R. Girshick, and A. Farhadi. You only look once: Unified, real-time object detection. In *Proceedings of the IEEE conference on computer vision and pattern recognition*, pages 779–788, 2016.
- [53] T.-Y. Lin, P. Goyal, R. Girshick, K. He, and P. Dollár. Focal loss for dense object detection. In *ICCV*, 2017.
- [54] C.-Y. Wang, A. Bochkovskiy, and H.-Y. M. Liao. Yolov7: Trainable bag-of-freebies sets new state-of-the-art for real-time object detectors. *arXiv:2207.02696*, 2022.

- [55] H. Zhang, F. Li, S. Liu, L. Zhang, H. Su, J. Zhu, L. Ni, and H. Shum. Dino: Detr with improved denoising anchor boxes for end-to-end object detection. In *International Conference on Learning Representations*, 2022.
- [56] M. Caron, H. Touvron, I. Misra, H. Jégou, J. Mairal, P. Bojanowski, and A. Joulin. Emerging properties in self-supervised vision transformers. In *Proceedings of the IEEE/CVF international conference on computer vision*, pages 9650–9660, 2021.
- [57] L. H. Li, P. Zhang, H. Zhang, J. Yang, C. Li, Y. Zhong, L. Wang, L. Yuan, L. Zhang, J.-N. Hwang, et al. Grounded language-image pre-training. In *CVPR*, 2022.
- [58] X. Zhou, V. Koltun, and P. Krähenbühl. Simple multi-dataset detection. In *CVPR*, 2022.
- [59] X. Wang, Z. Cai, D. Gao, and N. Vasconcelos. Towards universal object detection by domain attention. In *Proceedings of the CVPR*, pages 7289–7298, 2019.
- [60] H. Xu, L. Fang, X. Liang, W. Kang, and Z. Li. Universal-rcnn: Universal object detector via transferable graph r-cnn. In *AAAI*, 2020.
- [61] J. Redmon and A. Farhadi. Yolo9000: better, faster, stronger. In *Proceedings of the IEEE conference on computer vision and pattern recognition*, pages 7263–7271, 2017.
- [62] N. Bodla, B. Singh, R. Chellappa, and L. S. Davis. Soft-nms—improving object detection with one line of code. In *Proceedings of the IEEE international conference on computer vision*, pages 5561–5569, 2017.
- [63] Y.-T. Chen, J. Shi, Z. Ye, C. Mertz, D. Ramanan, and S. Kong. Multimodal object detection via probabilistic ensembling. In *ECCV*, 2022.
- [64] C. Guo, G. Pleiss, Y. Sun, and K. Q. Weinberger. On calibration of modern neural networks. In *ICML*, 2017.
- [65] Z. Yang, J. Chen, Z. Miao, W. Li, X. Zhu, and L. Zhang. Deepinteraction: 3d object detection via modality interaction. In *NeurIPS*, 2022.
- [66] J. Yan, Y. Liu, J. Sun, F. Jia, S. Li, T. Wang, and X. Zhang. Cross modal transformer: Towards fast and robust 3d object detection. *ICCV*, 2023.
- [67] R. Girshick, J. Donahue, T. Darrell, and J. Malik. Region-based convolutional networks for accurate object detection and segmentation. *IEEE transactions on pattern analysis and machine intelligence*, 38(1):142–158, 2015.
- [68] J. Deng, W. Dong, R. Socher, L.-J. Li, K. Li, and L. Fei-Fei. Imagenet: A large-scale hierarchical image database. In *CVPR*, 2009.
- [69] X. Zhou, R. Girdhar, A. Joulin, P. Krähenbühl, and I. Misra. Detecting twenty-thousand classes using image-level supervision. In *European Conference on Computer Vision*, 2022.
- [70] H. Zhang, P. Zhang, X. Hu, Y.-C. Chen, L. Li, X. Dai, L. Wang, L. Yuan, J.-N. Hwang, and J. Gao. Glipv2: Unifying localization and vision-language understanding. *NeurIPS*, 2022.
- [71] M. Minderer, A. Gritsenko, and N. Houlsby. Scaling open-vocabulary object detection. *arXiv:2306.09683*, 2023.
- [72] A. Madan, N. Peri, S. Kong, and D. Ramanan. Revisiting few-shot object detection with vision-language models. *arXiv preprint arXiv:2312.14494*, 2023.

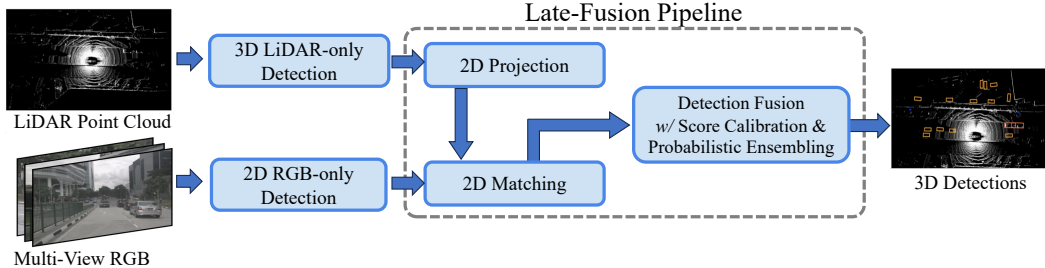


Figure 4: Our pipeline takes 3D LiDAR and 2D RGB detections as input (Fig.2A), matches 2D RGB and (projected) 3D LiDAR detections on the image plane (Fig.2B), and fuses matched predictions to generate improved 3D detections (Fig.2C).

A Implementation Details.

We include a pipeline diagram of our late-fusion approach above for clarity. We retrain several existing LiDAR-only, RGB-only, and multi-modal detectors on all 18 classes in the nuScenes LT3D setup. We employ standard augmentation techniques (such as copy-paste augmentation) and adopt the sampling ratios defined by [5] when training all detectors. Following established practices, we aggregate the past 10 sweeps for LiDAR densification using the provided ego-vehicle poses. We use the open-source implementations from [5] for training FCOS3D, CenterPoint, and TransFusion, and the first-party implementations for other detectors, following the training schedule proposed by each respective paper. We train our model with 8 RTX 3090 GPUs. By default, we train the 2D RGB detector with 2D bounding boxes derived from nuScenes’ 3D annotations and additionally train with 2D bounding boxes from nuImages where denoted. Our 2D RGB detectors, YOLOV7 and DINO, are pre-trained on the ImageNet [68] and COCO [50] datasets. We follow the default training recipes for both YOLOV7 and DINO respectively.

B Transformer-Based LiDAR Detectors

In the main paper, we evaluate all late-fusion methods by filtering LiDAR detections from CenterPoint with different RGB detectors for fair comparison to [5]. However, our late-fusion approach generalizes to other 3D LiDAR detectors as well. To this end, we evaluate our best-performing late-fusion configuration from the main paper with LiDAR detections from BEVFusion-L [6] and CMT-L [66] in Table 4.

First, we note that BEVFusion-L performs 2.1% better than CenterPoint on LT3D, notably improving on classes with few examples by 6.3%. However, BEVFusion-L performs 4.6% worse than CenterPoint on classes with many examples, suggesting that learning robust features for both common and rare categories is challenging. Surprisingly, CMT-L performs worse than CenterPoint on all classes. We find that filtering BEVFusion-L’s 3D detections with DINO’s 2D detections yields a fur-

Table 4: **Transformer-based 3D LiDAR detector.** We evaluate the late-fusion performance of BEVFusion-L and CMT-L (LiDAR-only) with DINO, and find that our late fusion strategy improves over BEVFusion-L by 8.2% overall and CMT-L by 15.9%. This suggests that our late-fusion approach generalizes across different 3D detector architectures.

Method	All	Many	Medium	Few
CenterPoint w/ Hier. [5]	40.4	77.1	45.1	4.3
CenterPoint w/ Hier. + DINO Det.	51.4	77.9	59.4	20.0
BEVFusion-L	42.5	72.5	48.0	10.6
BEVFusion-L + DINO Det.	50.7	76.8	59.1	19.1
CMT-L	34.7	73.4	35.9	1.1
CMT-L + DINO Det.	51.6	79.1	58.8	20.2
BEVFusion (RGB + LiDAR)	45.5	75.5	52.0	12.8
CMT (RGB + LiDAR)	44.4	79.9	53.0	4.8

Table 5: **NDS results.** We compare methods reported in the main paper w.r.t nuScenes Detection Score (NDS) and mAP. We find that the methods follow the same rankings on both metrics.

	FCOS3D [7]	BEVFormer [21]	CP [8]	TransFusion [31]	DeepInteraction [65]	CMT [66]	CP+FCOS3D [5]	CP+DINO (Ours)
mAP	20.9	27.3	39.2	39.8	43.7	44.4	43.6	51.4
NDS	30.4	38.8	54.9	53.9	54.4	55.9	56.7	60.4

Table 6: **Comparison of inference timing** (in ms). Our late-fusion approach runs faster than existing methods including end-to-end multimodal detectors such as DeepInteraction. Note that although our approach runs two uni-modal detectors, we run them in parallel so that the detection stage maintains the same efficiency as CenterPoint (CP). Moreover, our late-fusion strategy introduces negligible computation in inference. We copy 3D detection performance (in mAP) from Table 1 for reference, demonstrating that our simple late-fusion approach resoundingly outperform sophisticated state-of-the-art methods (e.g., Deep Interaction and TransFusion) with significantly less inference time!

	FCOS3D [7]	BEVFormer [21]	CP [8]	TransFusion [31]	DeepInteraction [65]	CP+FCOS3D [5]	CP + DINO (Ours)
Time (ms)	89	327	323	367	590	323	323
mAP	20.9	27.3	39.2	39.8	43.7	43.6	51.4

ther 8.2% improvement overall, and a 8.5% AP improvement for rare classes. This further supports our hypothesis that late-fusion with better 2D detectors can improve LT3D accuracy. In contrast, the end-to-end multi-modal variant of BEVFusion only improves over the LiDAR-only baseline by 3% overall, and performs 5.2% worse than our late-fusion approach. Similarly, filtering CMT-L’s 3D detections with DINO’s 2D detections yields a 15.9% improvement overall, with a 19.1% improvement for rare classes. Fusing CMT-L with DINO performs marginally better than CenterPoint with DINO.

We posit that the relative improvement from late-fusion can be attributed more generally to LiDAR-based detectors achieving high recall and low precision rather than the specific network architecture. Our late-fusion approach will be less effective for LiDAR-based detectors that achieve high precision and low recall since our method does not add new 3D detections (by lifting 2D detections), but rather only filters existing ones.

C AP vs. NDS Results

We report nuScenes Detection Score (NDS) and mAP results in Table 5. We find that all prior methods follow the same ranking on both metrics. This is unsurprising because NDS is computed as a weighted sum of mAP and other true positive metrics, where mAP is weighted five times greater than other components.

D Inference Runtime

Table 6 compares the inference runtime of our method against prior works on a single GPU. Although late-fusion methods such as our method (CP + DINO) and “CP + FCOS3D” [5] run two uni-modal detectors, we run them in parallel. Therefore, our final detector maintains the same runtime as a typical uni-modal detector and is often faster than more sophisticated multimodal detectors like BEVFormer [21], TransFusion [31] and DeepInteraction [65]. However, running two detectors in parallel will require more memory usage. Importantly, late-fusion methods including CP + DINO and [5] have negligible overhead when fusing uni-modal detections, hence their runtime is the same as CenterPoint, which serves as the speed bottleneck. This work uses research-level code and can be further optimized for deployment on autonomous vehicles.

E Per-Class Breakdown Results

We compare recent multi-modal methods w.r.t per-class AP in Table 7. All multi-modal methods perform similarly on common classes but considerably worse on Medium and Few classes, highlight-

Table 7: **Per-class performance on nuScenes.** Our late-fusion approach achieves the highest per-class AP on 5 out of 10 classes. Compared to DeepInteraction, our approach improves **construction worker** by 25.2%, **stroller** by 6.8%, and **pushable-pullable** by 27.3%. Note, CV is **construction vehicle**, MC is **motorcycle**, PP is **pushable-pullable**, CW is **construction-worker**, and **Stro.** is **stroller**. We highlight classes with Medium and Few examples per class in blue.

Method	Car	Adult	Truck	CV	Bicy.	MC	Child	CW	Stro.	PP
TransFusion [31]	84.4	84.2	58.4	24.5	46.7	60.8	3.1	21.6	13.3	25.3
BEVFusion [6]	90.2	67.2	65.5	35.2	58.8	77.0	4.4	39.0	29.6	34.1
DeepInteraction [65]	84.9	85.9	63.2	35.3	64.3	76.2	6.0	30.7	30.9	30.8
CMT [66]	88.6	87.7	65.2	36.9	66.7	76.3	4.7	34.4	9.4	34.1
CP + FCOS3D [5]	88.5	86.6	63.4	29.0	58.5	68.2	5.3	35.8	31.6	39.3
CP + DINO Det. (Ours)	86.3	86.2	60.6	35.3	70.1	75.9	8.8	55.9	37.7	58.1

Table 8: **Diagnosis using the mAP_H metric on selected classes.** We analyze CenterPoint and CMT with and without 2D late-fusion. Comparing the rows of LCA=0 for CenterPoint and CMT with and without late-fusion, we see our techniques bring significant improvements on classes with medium and few examples such as construction-vehicle (CV), bicycle, motorcycle (MC), construction-worker (CW), stroller, and pushable-pullable (PP). Moreover, performance increases significantly from LCA=0 to LCA=1 compared against LCA=1 to LCA=2, confirming that objects from rare classes are often detected but misclassified as some sibling classes.

Method	mAP_H	Car	Adult	Truck	CV	Bicycle	MC	Child	CW	Stroller	PP
CenterPoint (LiDAR-Only) <i>w/ Hierarchy</i>	LCA=0	88.6	86.9	63.4	25.7	50.2	63.2	0.1	25.3	8.7	36.8
	LCA=1	89.5	87.6	72.4	27.5	52.2	65.2	0.1	32.4	9.4	37.0
	LCA=2	89.6	88.0	72.5	27.7	53.2	65.7	0.1	34.0	9.8	37.6
CenterPoint <i>w/ Hier. + DINO Det.</i>	LCA=0	86.3	87.7	60.6	35.3	70.0	75.9	8.8	55.9	37.7	58.1
	LCA=1	86.8	88.3	68.5	37.3	70.4	77.1	16.2	66.0	51.5	58.2
	LCA=2	86.9	88.6	68.6	37.7	70.9	77.4	16.3	69.0	52.4	58.9
CMT (RGB + LiDAR)	LCA=0	88.6	87.7	65.2	36.9	66.7	76.3	4.7	34.4	0.9	34.1
	LCA=1	89.1	88.3	73.3	38.8	67.6	77.2	7.3	50.6	1.2	34.6
	LCA=2	89.1	88.6	73.4	39.0	68.3	77.7	7.7	52.6	1.3	35.6
CMT-L <i>+ DINO Det.</i>	LCA=0	87.1	87.3	62.7	35.3	72.0	76.1	11.9	53.9	29.6	56.4
	LCA=1	87.6	87.8	69.6	36.4	72.3	76.8	16.7	63.4	50.6	56.6
	LCA=2	87.6	88.1	69.7	36.7	72.7	77.3	16.9	66.3	53.2	57.3

ing the need for further investigation of LT3D by the research community. Notably, our late-fusion approach achieves 20% higher AP on pushable-pullable and 6% higher AP on stroller than prior work. In general, our late-fusion approach yields considerable improvement on classes with medium and few examples. Despite significant improvements in rare class detection accuracy, our approach detects child with a low 8% AP, which is still much better than compared methods. We posit that it is difficult to differentiate child from adult due to perspective geometry, since a small child close to the camera looks similar to a tall adult far away from the camera.

F Analysis of Misclassification

For 3D detection, localization and classification are two important measures of 3D detection performance. In practice, we cannot achieve perfect performance for either. In safety-critical applications, detecting but misclassifying objects (as a semantically related category) is more desirable than a missed detection (e.g., detect but misclassify a child as adult versus not detecting this child). Therefore, we evaluate CenterPoint and CMT using the hierarchical AP metric introduced by [5], which considers such semantic relationships across classes to award partial credit. Applying this hierarchical AP reveals that classes are most often misclassified as their LCA=1 siblings within coarse-grained superclasses.

Table 9: **Evaluating 2D detection performance.** We find that simply projecting 3D detections from RGB-only 3D detectors to 2D image plane yields considerably lower 2D detection mAP across all classes. However, 2D RGB detectors achieve higher performance. Intuitively, 2D RGB detectors achieve better classification performance and predict tighter fitting bounding boxes than those derived by projecting 3D detections to the image plane. This explains why fusing detections from 2D RGB detectors yields better LT3D performance than detections from 3D RGB detectors. All detectors in this table are only trained on the nuScenes train-set.

Method	All	Many	Medium	Few
FCOS3D (3D RGB Detector)	18.3	36.0	21.1	0.2
BEVFormer (3D RGB Detector)	23.0	40.8	28.2	2.1
PolarFormer (3D RGB Detector)	20.7	37.5	25.2	1.6
YOLOV7 (2D RGB Detector)	37.5	63.5	45.0	7.1
DINO (2D RGB Detector)	44.3	67.8	51.9	15.9

Table 10: **3D detection performance on the standard nuScenes benchmark.** We evaluate the impact of late-fusion for the standard nuScenes benchmark. Although our work focuses on improving detection accuracy in-the-tail, we find that our proposed approach can still improve detection accuracy for some common classes in the standard benchmark. Notably, fusing CenterPoint [8] with DINO [55] improves detection accuracy by 2.6% mAP and 6.9% NDS. However, fusing CMT [66] (a multi-modal 3D detector) with DINO [55] increases detection accuracy by 0.2%, only improving on *bicycle* and *traffic-cone*. We posit that CMT already effectively uses multi-modal training data for the (common) classes of the standard nuScenes benchmark, yielding diminishing returns with late-fusion. Note that CV stands for *construction vehicle*, MC represents *motorcycle*, and TC denotes *traffic cone*.

Method	Car	Truck	Trailer	Bus	CV	Bicy.	MC	Ped.	TC	Barrier	mAP	NDS
CenterPoint [8]	87.7	61.6	43.7	73.4	28.4	49.5	65.9	87.1	75.7	71.3	66.6	64.4
CenterPoint [8] + DINO Det.	86.2	60.1	44.6	76.1	35.3	70.0	75.9	86.6	81.5	74.6	69.2	71.3
CMT [66]	88.6	65.1	46.5	76.4	36.9	66.7	76.2	88.1	80.1	77.9	70.3	72.9
CMT [66] + DINO Det.	88.3	64.8	46.2	75.8	36.6	69.9	76.4	87.7	81.5	77.5	70.5	73.1

G Analysis of 2D Detection Performance

Table 9 shows that 2D detectors (e.g., DINO) outperform state-of-the-art 3D RGB detectors (e.g., BEVFormer) for 2D detection on the nuScenes val-set. Importantly, DINO performs significantly better than BEVFormer (15.9 vs. 2.1 mAP) on rare classes.

H Results on Standard nuScenes Benchmark

We evaluate our late-fusion method on the standard 10 classes of the nuScenes benchmark [2]. Although our late-fusion approach primarily improves performance for classes with *medium* and *few* examples per class, we find that the late-fusion of CenterPoint [8] and DINO [55] yields a 2.6% and 6.9% performance increase for mAP and NDS on the standard nuScenes benchmark, respectively. Notably, we see significant performance improvements for *bicycle* and *motorcycle*, likely because our LiDAR-only detector misclassifies these geometrically similar, but semantically different categories. Next We apply our late-fusion to CMT [66], a state-of-the-art multi-modal 3D detector, but find that our late-fusion approach only provides marginal performance improvements. Late-fusion of CMT [66] and DINO [55] only marginally improves *bicycle* and *traffic cone* performance. This suggests that CMT is already able to effectively utilize multi-modal information to correctly localize and classify common classes.

I Results on Argoverse 2

We present results on the large-scale Argoverse 2 (AV2) dataset developed for autonomous vehicle research. AV2 evaluates on 26 classes, which follow a long-tailed distribution. Following [5], we train on and evaluate detections up to 50m. As shown in Table 11, our main conclusions from nuScenes still hold for AV2. FCOS3D [7] yields poor performance on all classes, likely due to inaccurate depth estimates. CenterPoint performs considerably better, achieving high accuracy on classes with many examples. Notably, CenterPoint performs better on AV2’s rare classes (30.2 AP) compared to nuScenes’s rare classes (3.5 AP), likely because AV2 has more examples per-class in-the-tail. Lastly, our proposed late-fusion approach yields an 8.3% improvement over CenterPoint

Table 11: **Comparison with the Argoverse 2 state-of-the-art.** We present results on AV2 evaluated at 50m. FCOS3D [7] achieves poor performance, likely due to inaccurate depth estimates. In contrast, CenterPoint achieves strong performance on all classes. Our multi-modal fusion approach significantly improves over CenterPoint, achieving an 8.3% improvement averaged over all classes. These results on AV2 are consistent with those on nuScenes, demonstrating the general applicability of our approach.

Method	Modality	All	Many	Medium	Few
FCOS3D [7]	C	14.6	27.4	17.0	7.8
CenterPoint [8]	L	44.0	77.4	46.9	30.2
CenterPoint + FCOS3D [5]	C + L	48.4	79.0	51.4	35.3
CenterPoint + DINO Det. (Ours)	C + L	52.3	89.4	54.2	38.7

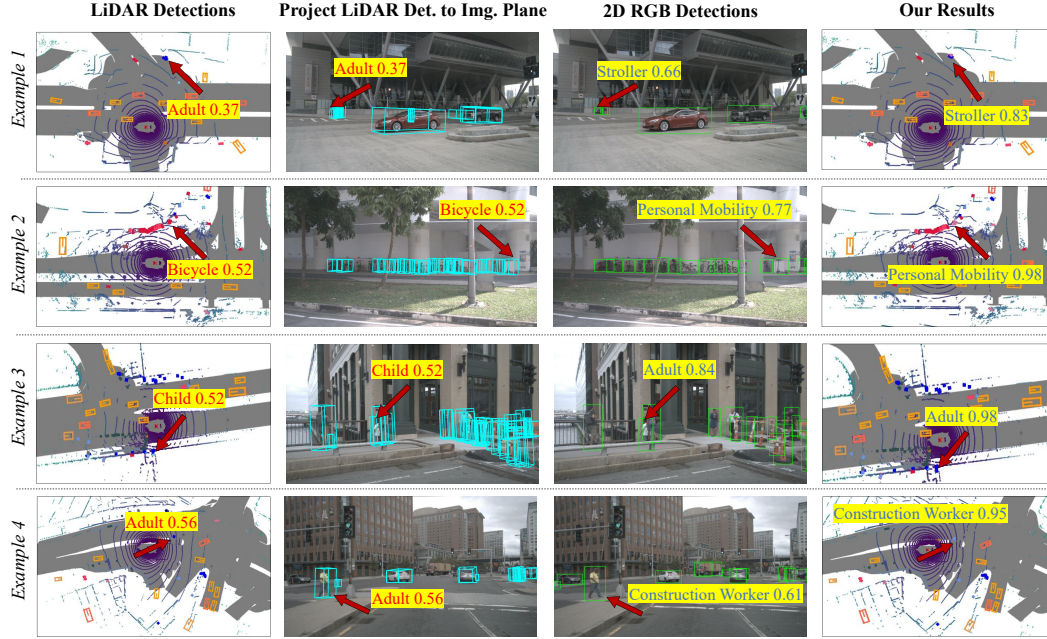


Figure 5: **Additional qualitative results.** We visualize the output of our late-fusion method which combines 3D LiDAR detections from CenterPoint and 2D RGB detections from DINO. In all cases, we find that the 2D RGB detector is able to correct classification errors from the 3D LiDAR detector, improving overall performance. Importantly, score calibration and probabilistic ensembling increases the confidence of the final prediction.

and a 3.9% improvement over prior work. These new results on AV2 are consistent with those on nuScenes, demonstrating the general applicability of our approach.

J More Visualizations

We present additional visualizations of our late-fusion approach in Fig. 5. Our method correctly classifies geometrically similar but semantically different categories like adult-vs-stroller, bicycle-vs-personal mobility, child-vs-adult, and adult-vs-construction worker. We provide a video of our results in the supplement.

Failure cases. We visualize common failure cases of our late-fusion approach and compare them with the failure cases of TransFusion [31], an end-to-end trained multi-modal detector. We find that our method fails in cases of occlusions (where there is no 3D information) and in cases where the 2D RGB detector misclassifies the object. See Fig. 6 for detailed analysis.

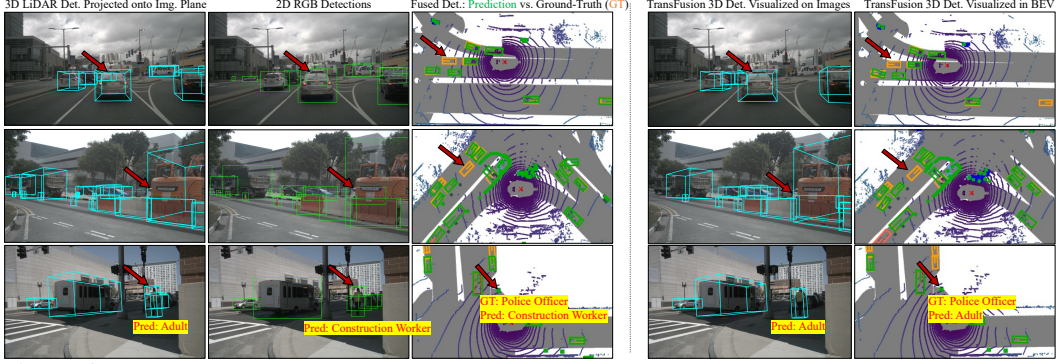


Figure 6: **Examples of failure cases.** Both our method (columns 1-3) and TransFusion [31] (columns 4 - 5) share the same failure cases. In the first and second row, the 2D RGB detector DINO detects the heavily occluded cars but 3D LiDAR detector fails to detect them. As a result, the late-fusion predictions miss these cars because our method throws away unmatched RGB detections since we do not have accurate 3D information. In the third row, we see that although both the LiDAR and RGB detectors fire on the object (whose ground-truth label is police-officer), the LiDAR detector classifies it as adult and RGB detector classifies it as construction-worker. As a result, the final detection is incorrect w.r.t the predicted categorical label. TransFusion also misclassifies this object as an adult.

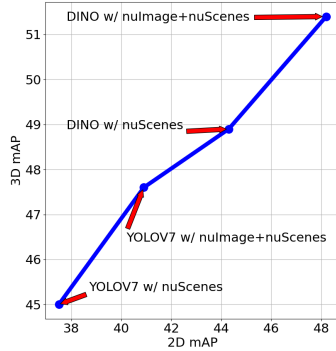


Figure 7: **Impact of 2D detector performance on LT3D.** While nuScenes is a 3D detection benchmark, we can generate 2D annotations using the provided sensor extrinsics by projecting the 3D annotations onto the 2D image plane. Results show that evaluating 2D detectors using these 2D annotations is a good proxy task (x-axis) that is positively correlated with the downstream 3D detection performance of the full late-fusion pipeline (y-axis). Concretely, training 2D detectors with more data (e.g., training with nuScenes + nuImages vs. nuScenes only) and using better 2D detectors (e.g., DINO vs. YOLO-v7) improve performance on the proxy task of 2D detection and the downstream 3D detection achieved by our late-fusion algorithm.

K Limitations and Future Work

Our work focuses on LT3D, a problem that emphasizes 3D object detection for rare classes like stroller and debris, which are often safety-critical for AVs. Therefore, improving LT3D is important for ensuring safe autonomy. However, our work does not directly study how addressing LT3D affects downstream perception tasks. Future work should address this limitation. Moreover, as shown in Fig. 7, simply training better 2D RGB detectors with more data provides a natural pathway for improving LT3D performance. We find that 2D detection accuracy on nuScenes is a strong proxy for final 3D LT3D performance. Recent works in large-scale vision language models [69, 70, 71, 72] show promising zero-shot results in detecting rare classes. Identifying ways of incorporating foundation models into our late-fusion framework might improve LT3D further.

In addition, our proposed late-fusion approach is unlikely to work well for objects that are visible in LiDAR but occluded in RGB images (or visible in RGB images but occluded in LiDAR, but this is unlikely because LiDARs are typically mounted higher than RGB cameras). Notably, due to LiDAR and RGB sensors not being co-located on the autonomous vehicle, some objects may be visible in one modality but occluded in another. If an object is visible in LiDAR but not in RGB, we would down-weight the confidence scores of LiDAR-based detections that not supported by RGB-based detections. In contrast, if an object is visible in RGB but not in LiDAR, our 2D late-fusion pipeline would not be able to detect this object in 3D.

Next, we note that the success of late-fusion requires good sensor calibration between the RGB cameras and LiDAR sensor. In fact, sensor calibration errors can also affect early- and mid-fusion

methods as they require calibrated extrinsics [22]. As publicly available datasets (e.g., nuScenes and Argoverse 2) are collected in real-world scenarios, one may assume that such datasets *already* capture realistic calibration errors. Nevertheless, studying how sensor calibration errors affects LT3D performance is worthy of further exploration in future work, which requires collecting new datasets by controlling for such errors.

Lastly, we note that although our proposed approach is highly relevant to 3D perception for autonomous vehicles, our work does not evaluate on real robots. However, following prior literature, evaluating on nuScenes and Argoverse 2 serves as a well established proxy for performance in-the-wild.